Supporting Information

Takesono et al. 10.1073/pnas.1200642109

SI Materials and Methods

Multiphoton Microscopy. Two-photon fluorescence (TPF) and coherent anti-Stokes Raman scattering microscopy (CARS) were performed simultaneously using a custom-built multimodal imaging system (1, 2). Excitation was provided by Optical Parametric Oscillator (Levante Emerald; APE-Berlin) pumped with a frequency-doubled Nd:Vanadium picosecond oscillator (High-Q Laser Production GmbH). The optical parametric oscillator uses noncritically phased matched optical parametric generation to produce pulsed signal and idler beams with a perfect temporal overlap with a repetition rate of 76 MHz and 6-ps pulse width. Continuous tuning over a wide range of wavelengths is available (670–980 nm for the signal and 1,130–1,450 nm for the idler output). Signal and idler wavelengths of 924 and 1255 nm, respectively, were used to provide CARS contrast of the asymmetric CH_2 mode at 2,855cm^{-1} found abundantly in lipids. The signal beam at this wavelength (924 nm) was used for simultaneous two-photon excitation of the GFP.

Imaging was performed using a modified commercial inverted microscope and confocal laser scanner (IX71 and FV300; Olympus). Home-built external detectors containing red-sensitive photomultiplier tubes (R3896; Hamamatsu) were used to detect the CARS and TPF signals. CARS was detected in the forward direction via an air condenser (NA = 0.55) and was spectrally isolated from the excitation and TPF by a band-pass filter centered at 750 nm (HQ750/210; Chroma Technologies). TPF was detected in the epi-direction via a long-wave-pass dichroic mirror (z850rdc-xr; Chroma Technologies) to separate the signal from the excitation beams, and band-pass filters (CG-BG-39–1.00–1 and F70-500–3-PFU; CVI) were used to isolate the GFP emission spectrally. All imaging was performed using a 60× 1.2 NA water-immersion objective (UPlanS Apo; Olympus) and the minimal possible laser power to avoid damage to the samples.

Plasmid Constructions. ***HN-slc3a2-b.*** The cDNA of *HN-slc3a2-b* was generated by PCR. The cDNA for the intracellular domain of HPIV-2 HN (*IC-HPIV-2 HN*) was amplified from human HN-FRP-1/CD98hc cDNA (3) using the primer pair 5′-GCGGATCCGCCGCCATGGAAGATTACAGCAATCTA-3′ and 5′-GCGAATTCTCGGAAAATGATTCTA-3′. Then the cDNA fragment of zebrafish Slc3a2-b (accession no. BC044497) lacking the first 29 amino acids of its intracellular domain (Δ*IC-slc3a2-b*) was amplified from pBluescript-*slc3a2-b*. Both fragments were subcloned into pCS2+ using BamH1/EcoR1 and EcoR1/Xho1, respectively, to generate pCS2-*HN-slc3a2-b*.

Zebrafish RhoA. Full-length RhoA-b cDNA (accession no. BC075938) was purchased from Open Biosystems, and RhoA-b cDNA was amplified by PCR using the primer pair 5′-ATCTCGAG GCCACCATGGCAGCAATTCGCAAG-3′ (RhoA-b-forward primer) and 5′-ATTCTAGAATTCACAGCAGACAGCATTTGTTG-3′ (RhoA-b-reverse primer) and was subcloned into pCS2+ to generate pCS2-RhoA-b.

Zebrafish RhoA-b-G14V. RhoA-b G14V cDNA was generated by two-step PCR. First, two cDNA fragments containing a point mutation for Glycine 14 to Valine were generated from pCS2-RhoA by PCR using two primer pairs: (*i*) RhoA-b forward primer and 5′-TTC CCG CAT GCT ACA TCT C-3′ (RhoA-b G14V reverse primer) and (*ii*) 5′-AGG AGA TGT AGC ATG CGG G-3′ (RhoA-b G14V forward primer) and RhoA-b reverse primer. The PCR products from *i* and *ii* were pooled and used as a template for the second PCR using the primer pair of RhoA-b foward primer and RhoA-b reverse primer to generate the full-length RhoA-b-G14V. RhoA-b-G14V cDNA was subcloned into pCS2+. All synthesized cDNAs were confirmed by sequencing (Eurofins; MWG).

pCS2-GFP-FL-v-Src. pCS2-GFP-FL-v-Src was kindly provided by Yasuyuki Fujita (Hokkaido University, Sapporo, Japan).

1. Moger J, Johnston BD, Tyler CR (2008) Imaging metal oxide nanoparticles in biological structures with CARS microscopy. *Opt Express* 16(5):3408–3419.
2. Mansfield J, et al. (2009) The elastin network: Its relationship with collagen and cells in articular cartilage as visualized by multiphoton microscopy. *J Anat* 215(6):682–691.
3. Okamoto K, et al. (1997) Paramyxovirus-induced syncytium cell formation is suppressed by a dominant negative fusion regulatory protein-1 (FRP-1)/CD98 mutated construct: An important role of FRP-1 in virus-induced cell fusion. *J Gen Virol* 78(Pt 4): 775–783.

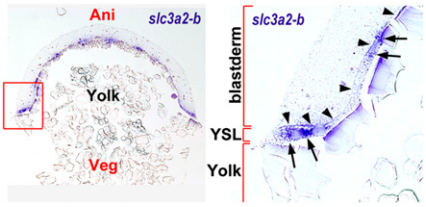

Fig. S1. Zebrafish *slc3a2* is expressed specifically in the yolk syncytial layer (YSL). Shown is a section of 50% epiboly-stage embryo stained by whole-mount in situ hybridization using the *slc3a2-b* probe. (*Left*) Vertical section of the whole embryo. (*Right*) Enlarged view of the section of the blastoderm rim outlined in the left panel. *slc3a2-b* expression is restricted at the YSL (arrowheads indicate the border between the blastoderm and the YSL) and accumulates around the yolk syncytial nuclei (YSN) (indicated by arrows).

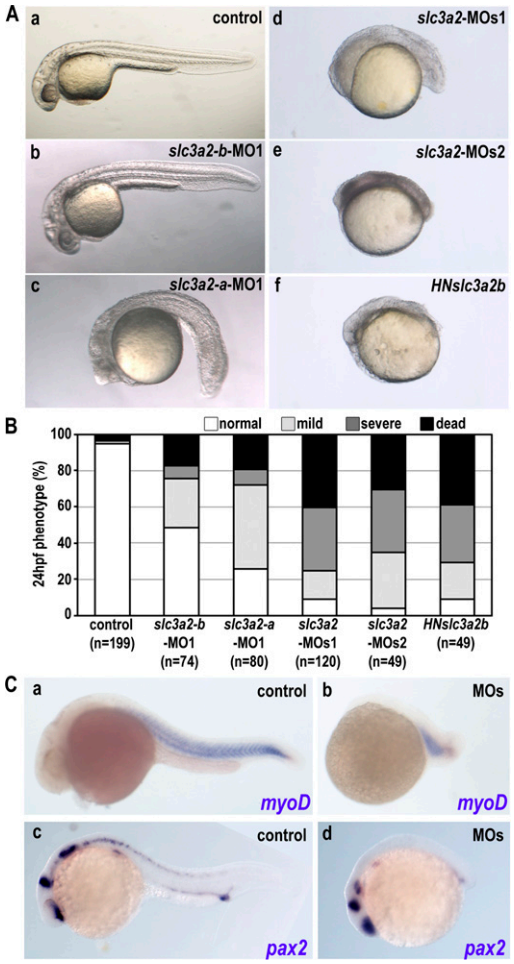

Fig. S2. Loss of function of Slc3a2 induces morphological defects but does not affect patterning. (*A*) Morphological phenotypes caused by *slc3a2* knockdown. (*a*) Control embryo. (*b*–*e*) Morphant embryo injected with *slc3a2-b*-MO1 (*b*); *slc3a2-a*-MO1 (*c*); a combination of *slc3a2-a*-MO1 and *slc3a2-b*-MO1 (*slc3a2*-MOs1) (*d*); or a combination of *slc3a2-a*-MO2 and *slc3a2-b*-MO2 (*slc3a2*-MOs2) (*e*). (*f*) Embryo overexpressing *HN-slc3a2-b* (HNslc3a2b) (*Material and Methods*). Single-gene knockdown by morpholino causes mild phenotypes (*b* and *c*), whereas double knockdown of both *slc3a2-a* and *slc3a2–b* by a set of MO1 or MO2 (*d* and *e*) or overexpression of *HN-slc3a2-b* (*f*) induces severe morphological defects with a smaller head and shorter tail. Images are 1-day-old embryos. (*B*) Phenotypes at 24 h postfertilization were categorized as normal (white), mild (light gray), severe (small head and short body axis) (dark gray), or dead (black). Representatives of mild and severe phenotypes in morphants are shown in Fig. 1*B*. Data shown are from three experiments, and the total number of embryos is shown below each bar. (*C*) Whole-mount in situ analyses for *MyoD* (*a* and *b*) and *pax2* (*c* and *d*) in control and *slc3a2*-morphants (MOs). Note that expression patterns of *MyoD* and *pax2* are retained despite severe morphological changes.

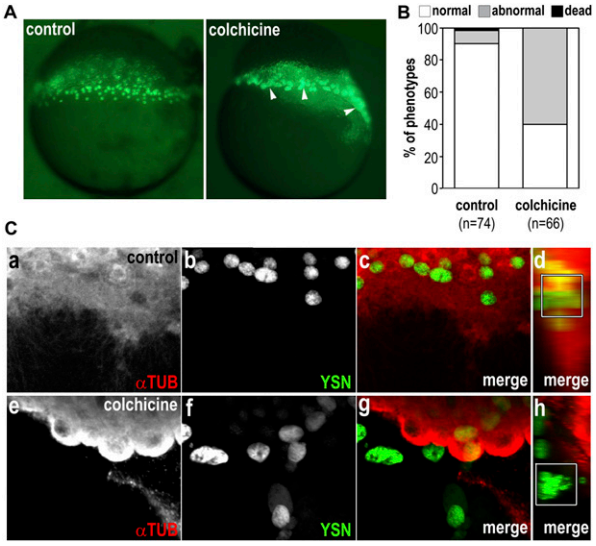

Fig. S3. Microtubule depolymerization alters YSL organization. (*A*) The YSN are visualized by Sytox green. Shown are lateral views of dome-stage embryos from control and an embryo treated with 10 μM colchicine from the 32-cell stage. Clustered YSN are indicated by white arrowheads. (*B*) At the dome stage, the embryo phenotype is categorized as normal (showing uniform distribution of the YSN without YSL deformation/expansion) (white), abnormal (showing altered YSN localization including uneven distribution of the YSN and YSN clustering with YSL deformation/expansion) (gray), or dead (black). Data are from more than three different experiments. Total number of embryos is shown below each bar. (C) Microtubule networks are shown by α-tubulin antibody staining (*a* and *e*), and the YSN is shown by *sytox* green (*b* and *f*). Merged images of α-tubulin (red) and Sytox green (green) (*c* and *g*) and reconstituted section views of the merged images rotated by 90° (*d* and *h*) are shown. Control shows overlap of the YSN and dense YSL microtubule networks (white square in *d*) missing in colchicine-treated embryo (*h*).

Table S1. Phenotypes of embryos injected with Sytox green

Embryos	Normal (%)	Abnormal (%)	Dead (%)
Control (*n* = 191)	91.4 ± 1.7	6.7 ± 1.3	1.9 ± 0.2
MOs (*n* = 195)	20.5 ± 2.4	74.9 ± 3.4	4.6 ± 1.1
HNslc3a2b (*n* = 61)	21.6 ± 1.1	75.8 ± 1.5	2.6 ± 0.6
G14V (*n* = 114)	0.6 ± 0.2	62.7 ± 5.0	36.8 ± 9.6
MOs+slc3a2b (*n* = 97)	53.6 ± 8.9	37.9 ± 4.9	8.6 ± 2.2
MOs+RhoAMO (*n* = 133)	67.8 ± 6.3	23.3 ± 2.7	8.9 ± 1.6
MOs+Y27632 (*n* = 143)	60.3 ± 3.8	27.1 ± 3.5	12.6 ± 1.3
MOs+v-Src (*n* = 65)	75.6 ± 5.1	17.9 ± 6.6	6.5 ± 1.5
slc3a2-b-MO2 (*n* = 121)	37.9 ± 4.9	59.7 ± 5.6	2.3 ± 0.3
slc3a2-b-MO2+slc3a2b (*n* = 75)	62.5 ± 6.2	22.9 ± 4.6	14.6 ± 3.1

Data are from at least three different experiments. *n* = total number of embryos.

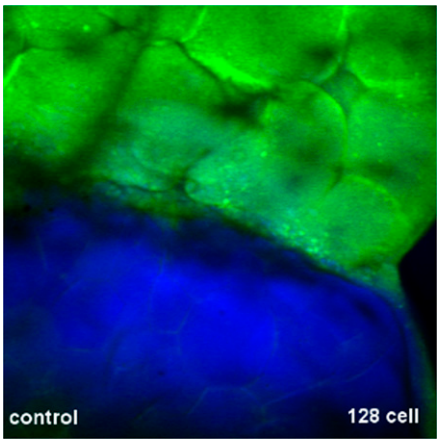

Movie S1. Time-lapse movie (2 min per frame) of TPF (for GFP membrane) and CARS (for lipids) images in a developing control embryo. Arrows indicate the position of cell–cell fusion at the marginal blastomeres during the transition between the 512-cell stage to the 1k-cell stage. Note that the positions of the YSN are mostly stationary.

Movie S1

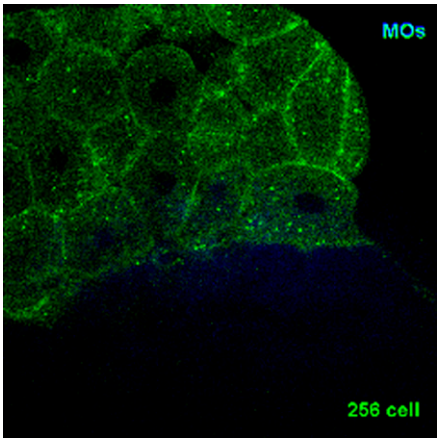

Movie S2. Time-lapse movie (2 min frame) of TPF (for GFP membrane) and CARS (for lipids) images in a developing *slc3a2*-MOs embryo. Numbered green arrows (1–4) indicate the positions of cell–cell fusion during the period from the 512-cell stage to the oblong stage. Blue arrows indicate the position of two clustered nuclei over the period of image acquisition, demonstrating the quick movement of the nuclei within the YSL.

Movie S2

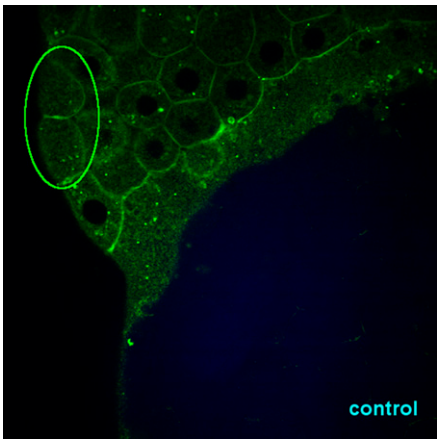

Movie S3. Time-lapse movie (2 min/frame) of TPF (for GFP membrane) and CARS (for lipids) images in a developing control embryo. Green circle highlights the two EVL cells, which undergo cell–cell fusion (indicated by arrows).

Movie S3